Available online at www.sciencedirect.com
ScienceDirect
Trans. Nonferrous Met. Soc. China 34(2024) 2476−2490
Transactions of Nonferrous Metals Society of China
www.tnmsc.cn

Cross-section distortion and springback characteristics of double-cavity aluminum profile in force controlled stretch-bending

Zhi-wen LIU[1,2], Zi-xuan DONG[1], Cong-chang XU[2], Jie YI[2], Luo-xing LI[2]

1. School of Mechanical Engineering, University of South China, Hengyang 421001, China;
2. State Key Laboratory of Advanced Design and Manufacturing Technology for Vehicle, Hunan University, Changsha 410082, China

Received 26 June 2023; accepted 6 December 2023

Abstract: A 3D elastic-plastic FE model for simulating the force controlled stretch-bending process of double-cavity aluminum profile was established using hybrid explicit−implicit solvent method. Considering the computational accuracy and efficiency, the optimal choices of numerical parameters and algorithms in FE modelling were determined. The formation mechanisms of cross-section distortion and springback were revealed. The effects of pre-stretching, post-stretching, friction, and the addition of internal fillers on forming quality were investigated. The results show that the stress state of profile in stretch-bending is uniaxial with only a circumferential stress. The stress distribution along the length direction of profile is non-uniform and the maximum tensile stress is located at a certain distance away from the center of profile. As aluminum profile is gradually attached to bending die, the distribution characteristic of cross-section distortion along the length direction of profile changes from V-shape to W-shape. After unloading the forming tools, cross-section distortion decreases obviously due to the stress relaxation, with a maximum distortion difference of 13% before and after unloading. As pre-stretching and post-stretching forces increase, cross-section distortion increases gradually, while springback first decreases and then remains unchanged. With increasing friction between bending die and profile, cross-section distortion slightly decreases, while springback increases. Cross-section distortion decreases by 83% with adding PVC fillers into the cavities of profile, while springback increases by 192.2%.
Key words: hollow aluminum profile; force controlled stretch-bending; numerical parameters; springback analysis approach; cross-section distortion; springback; process parameters

1 Introduction

Aluminum profiles are widely used in automobile industry due to their light mass, high specific strength and stiffness, and good energy absorption [1−4]. Considering the requirements for aerodynamics, structural mechanics and aesthetics, automotive aluminum profiles need to be bent into certain curvatures, thus placing high demands on their dimensional accuracy and performance. The manufacturing of curved profiles is mostly achieved through two key forming processes. Firstly, an aluminum billet is extruded into a straight profile with certain cross-section [5−8]. Then, the semi-finished straight profile is bent into a curved shape using an external bending device. In recent decades, various techniques for bending straight profiles have been developed, such as press bending [9], roll bending [10], stretch-bending [11] and rotary draw bending [12]. Among them, stretch-bending is the most feasible and efficient method due to its outstanding advantages of low cost and good reproducibility. Stretch-bending can be classified

Corresponding author: Zhi-wen LIU, Tel: +86-15874949745, E-mail: liuzhiwen1008@163.com;
Luo-xing LI, Tel: +86-731-88821571, E-mail: luoxing_li@yahoo.com
DOI: 10.1016/S1003-6326(24)66554-4

into displacement control and force control methods based on the control system used. When loading in displacement mode, the elongation of profile can be accurately controlled by the movement trace of the jaw gripper, while in force loading mode, the stretching force applied to the profile can be precisely controlled. Cross-section distortion and springback are two most common forming defects in stretch-bending of hollow profiles [13], which seriously affect the dimensional accuracy and assembly quality of the product. Compared with steel components, aluminum ones have a higher ratio of material strength to Young's modulus, making it more difficult to avoid and control these defects in stretch-bending.

Recently, analytical methods have been extensively applied to studying the stress, strain distributions and deformation behaviors of aluminum profile in stretch-bending. EL-DOMIATY and ELSHARKAWY [14] proposed a mathematical model to determine the springback as a function of material, geometric parameters and forming load in stretch-bending of a U-shaped profile. ZHU and STELSON [15] developed an analytical expression for the cross-section distortion of rectangular tube in stretch-bending based on the upper bound theory of plasticity and energy minimization. CORONA [16] proposed a formula to predict the springback and cross-section distortion of aluminum profile in bending-stretching considering the impacts of tension and internal pressure. YU and LI [17] established the theoretical model to characterize the springback of a L-type profile in rotary stretch bending based on the stress and strain distributions of the cross-section. ZHAO et al [18] and ZHAI et al [19] developed a universal analytic model for solving the springback of rectangular and U-section profiles in plane stretch-bending based on the classical elastic-plastic theory and the characteristic of strain superposition. MA and WELO [20] proposed a full moment analytical framework for springback assessment in flexible stretch-bending of aluminum square profile. The analytical method is mainly based on the simplified process and material properties, which has certain limitations for complex hollow profiles. However, the cross-sectional shape of the profile directly affects the stress and strain distributions in stretch-bending. Thus, analytical method is commonly applied to investigating the bending deformation behaviors of aluminum profiles with simple shapes.

At the same time, some researchers have studied the springback and cross-section distortion behaviors in stretch-bending through experimental methods. MILLER et al [21] developed a custom bend−stretch−pressure testing facility that can monitor the cross-section variation of aluminum tube. LIU et al [22] investigated the springback behaviors of age-hardened Al−Li alloy profiles during displacement controlled stretch-bending. The effects of material, bending radius and stretching strain on springback were revealed. CLAUSEN et al [23] experimentally studied the stretch-bending process of two generic aluminum bumper sections. The effects of six different stretch-bending procedures on forming quality of profiles were investigated. LIU et al [24] carried out an experimental study on the hot stretch-bending of T-section extruded profile. They also experimentally investigated the three types of failures occurring in the stretch-bending of aluminum profiles [25]. It is time-consuming and laborious to carry out the stretch-bending analysis using experimental method, which is mainly used to verify the accuracy of theoretical or finite element (FE) models.

Considering the geometric, material and contact nonlinearities, stretch-bending is a complex incremental forming process under the coupling effects of multi-factors. As a consequence, it is difficult to solve the actual problems accurately and effectively through analytical or experiment methods. In comparison, FE method is a well-established tool for analyzing the complicated stretch-bending process and predicting the appearance of forming defects. PAULSEN and WELO [26] numerically investigated the effects of cavity number, material and bending radius on the cross-section distortion and springback in the stretch-bending of rectangular profile. HOPPERSTAD et al [27] evaluated the sensitivity of local deformation of aluminum profile to the shape of yielded surface and plastic anisotropy of material in stretch-bending using FE simulations. GU et al [28] investigated numerically the stretch-bending process of Z-type profiles and revealed the induced mechanisms of the cross-section distortion and poor contour precision. LIU et al [29] analyzed the effect of post-stretching on the deformation behavior of aluminum hollow profile in stretch-bending through numerical simulations. LIANG et al [30] numerically

simulated the flexible multi-points stretch-bending process of a complex 3D part and studied the influence of process parameters on springback. GU et al [31] revealed the causes of wrinkling and cross-section distortion during the stretch-bending of L-section variable−curvature profiles. To sum up, much research has been conducted on the prediction and control of forming defects in the displacement controlled stretch-bending of aluminum profiles by FE analysis methods, which can provide useful references for understanding and studying the force controlled stretching-bending. However, in industrial production, forming defects in force controlled stretch-bending of high strength hollow aluminum profiles with complex cross-sections are still solved by the engineers' experiences or time-consuming trials. Thus, accurate analysis and optimization of force controlled stretch-bending using FE simulation is an important research hotspot in aluminum profile manufacturing.

In this work, a 3D elastic-plastic FE model for simulating the force controlled stretch-bending process of a double-cavity aluminum profile was established using hybrid explicit-implicit solvent method. Considering the computational accuracy and efficiency, the optimal choices of numerical parameters and algorithms in FE modelling were determined. The effective and principal stresses of the bending profile in the global coordinate system and the 3D stresses in the local cylindrical coordinate system were quantitatively analyzed. The formation mechanisms of cross-section distortion and springback were revealed. The effects of pre-stretching, post-stretching, friction, and addition of internal fillers on forming quality were systematically investigated. This study can provide valuable references for accurate FE modeling of stretch-bending process and determining the appropriate process conditions in forming operation.

2 Force controlled stretch-bending process

2.1 Process principle and forming device

The research object in this study was a double-cavity aluminum profile applied in the front bumper beam of an automotive body. Figure 1 shows the cross-section shape and dimensions of the curved profile. Its cross-section shape is asymmetrical, with a large width/height ratio and unequal wall thickness. As shown in Fig. 2, the curved profile is manufactured using a force controlled stretch-bending process, which consists of three forming stages: pre-stretching, bending, and post-stretching. The important process factors in stretch-bending include pre-stretching and post-stretching forces, friction between bending die and profile, and adding fillers in profile cavity. The forming experiments were carried out on an SBL−30ZD−6 type machine with a maximum stretching load of 35 t. The initial length of aluminum profile in stretch-bending was set to be 1345 mm.

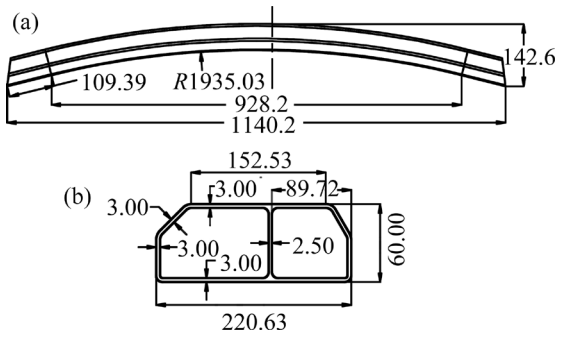

Fig. 1 Cross-sectional shape and dimensions of double-cavity aluminum profile: (a) Over size of bending profile; (b) Cross-sectional dimensions (Unit: mm)

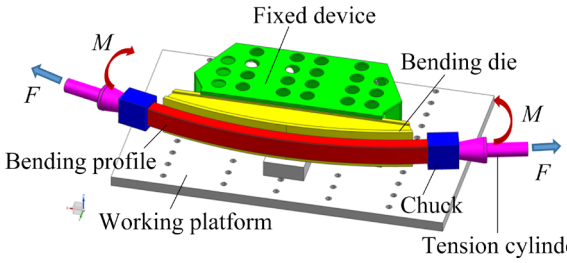

Fig. 2 Forming principal and device in force controlled stretch-bending of aluminum profile (F represents pre- and post-stretching forces, and M is bending moment)

2.2 Criteria for evaluating forming quality

Cross-section distortion and springback always accompany the bending of hollow profile, leading to product failure. The cross-section distortion in bending is mainly manifested by the collapse of upper flange and slight concave of the lower flange. In this study, 17 cross-sections were intercepted along the length direction of bending profile and the collapse values (ΔH) of upper flanges on all cross-sections were measured (see Fig. 3(a)). The total arc length of bent profile was defined as L_0.

Taking the middle cross-section $C1$ as the reference and the arc length from cross-section Cn (n=2−9, 2′−9′) to the middle cross-section $C1$ was defined as L. L/L_0 indicates the location of cross-section Cn along the length direction of bending profile. The location range between cross-sections $C9$ and $C9'$ along the length direction of bending profile is from −0.5 to 0.5.

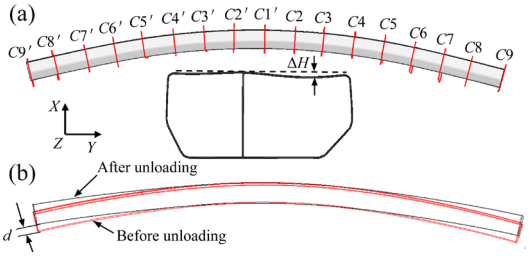

Fig. 3 Evaluation indexes of forming quality for double-cavity profile: (a) Definition on cross-section distortion and measuring positions along length direction of bent profile; (b) Definition on springback

Springback is also an unavoidable problem in the stretch-bending of hollow profile. Excessive springback results in serious dimensional deviation of curved profile. Springback can be characterized by the curvature variation, springback angle, and normal displacement before and after bending. In this study, the springback of curved profile was evaluated by the normal displacement d at both ends of profile, as shown in Fig. 3(b).

3 FE modelling

3.1 Meshing technique

A FE mesh model for simulating the force controlled stretch-bending process of the double-cavity aluminum profile was established based on the ANSA and LS-DYNA software (see Fig. 4). The mesh model consisted of five parts, including the profile, bending die, chuck, rotating arm, and PVC fillers. The aluminum profile was defined as an elastic-plastic material, while the bending die and tools were defined as rigid material. The aluminum profile was a typical thin-shell structure and meshed using 4-node shell elements. The PVC fillers were meshed by with 8-node hexahedron elements with element size of about 6 mm. The tools and bending die were meshed using 4-node shell elements and the element size was set to about 8 mm. Shell element formulation, element size and the number of through-thickness integration points (NIP) are three important factors directly relating to the stiffness and stress−strain solution of elements. Therefore, how these numerical parameters and algorithms affect the computational accuracy and efficiency needs to be studied.

3.2 Material models

Material constitutive relationships between double-cavity aluminum profile and PVC fillers have significant impacts on the simulated accuracy. The material of double-cavity profile is a 6063 aluminum alloy. After porthole die extrusion, the extruded profile was water-cooled, and then heat-treated at 180 °C for 4 h. Since the stretch-bending process can be considered as a quasi-static process, stress−strain behavior of the material can be obtained by tensile test. Figure 5 shows the true stress−strain curve of aluminum profile at tensile rate of 3 mm/min. A power exponential material model was applied to describing the deformation behavior of aluminum profile in stretch-bending process, which is expressed in Eq. (1):

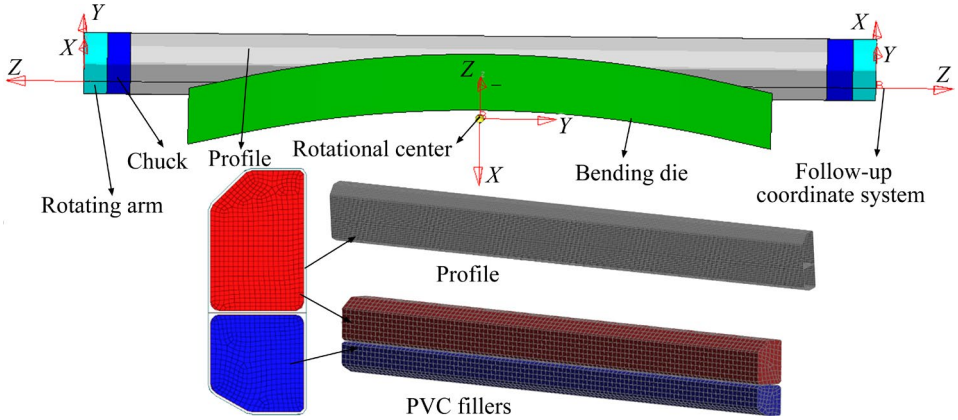

Fig. 4 FE mesh model of force controlled stretch-bending process

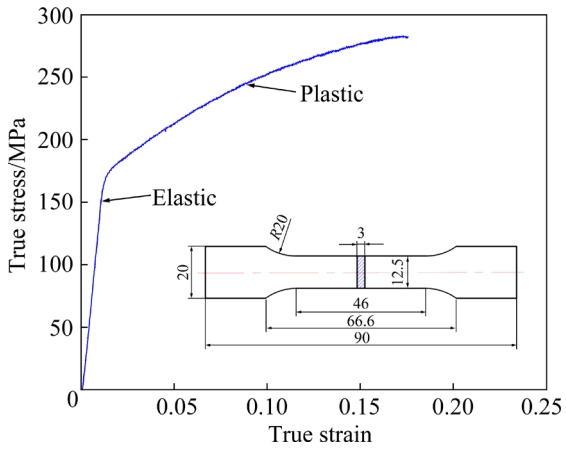

Fig. 5 True stress−strain curve of double-cavity aluminum profile (Unit: mm)

$$|\sigma|=\begin{cases}E|\varepsilon|, \text{ if } |\sigma|\le\sigma_0\\ K|\varepsilon|^n, \text{ if } |\sigma|>\sigma_0\end{cases} \quad (1)$$

where σ is the yield stress, ε is the strain, E is the Young's modulus, σ_0 is the initial yield stress, and K and n are the strengthening coefficient and strain hardening index, respectively. These parameters were determined by fitting the experimental stress−strain curve, such as σ_0=170.3 MPa, K=351.296 MPa, n=0.10422, and E=79.8 GPa.

The material behavior of PVC fillers can be characterized by a nonlinear super-elastic material model, which is defined by the strain energy. Assuming that the filler material is isotropic and deformation is incompressible, the constitutive model can be described as follows:

$$W=W(I_1,\ I_2,\ I_3) \quad (2)$$

where W is the strain energy, and I_1, I_2 and I_3 are the invariants of deformation tensors, $I_1=\lambda_1^2+\lambda_2^2+\lambda_3^2$, $I_2=\lambda_1^2\lambda_2^2+\lambda_2^2\lambda_3^2+\lambda_3^2\lambda_1^2$, $I_3=\lambda_1^2\lambda_2^2\lambda_3^2$, $\lambda_i=1+\gamma_i$; λ_1, λ_2 and λ_3 are the main extension ratios, and γ_i is the principal strain of deformation.

The Mooney−Rivlin constitutive model was applied to describing the strain energy density function, which was expressed with a typical quadratic third-order equation, as shown in Eq. (3):

$$W=C_{10}(I_1-3)+C_{01}(I_2-3)+(1/a)(J-1)^2 \quad (3)$$

where C_{10}, C_{01} and a are material constitutive parameters, which can be determined by fitting test compression curves. J is the elastic volume ratio, and when the material deformation behavior is incompressible, J=1.

There are two ways to define the Mooney−Rivlin model. The first method is to directly use the compressive stress−strain curve as an input material data in FE modelling, and the second option is to determine the constitutive parameters of material. In this study, the first method was used to simulate the deformation behavior of PVC fillers in the stretch-bending process. The compressive stress−strain curve of the material was obtained by a uniaxial compression test, and then dealt using 3-order smoothing, as shown in Fig. 6.

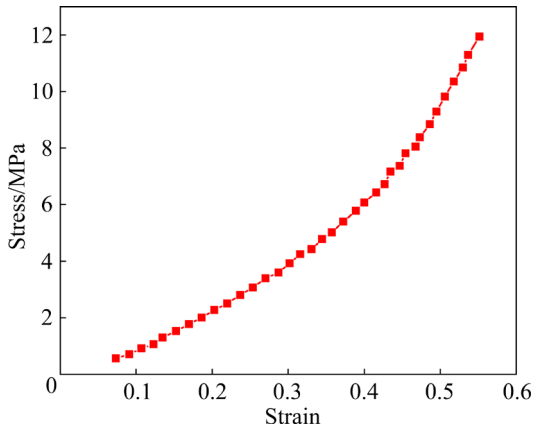

Fig. 6 Uniaxial compressive stress−strain curve for PVC fillers

3.3 Process and contact conditions

The bending die was fixed on the working platform, thus all degrees of freedom were constrained. Pre-stretching or post-stretching forces were exerted on the aluminum profile by a local coordinate system, so that the direction of stretching forces always follows the normal direction of profile cross-section during bending. The bending moment was exerted by rotating arms using the keyword command *Boundary_prescribed_motion_velocity. The contact between the aluminum profile and the bending die is modeled using the forming-one-way-surface-to-surface algorithm, while that between the aluminum profile and PVC fillers is modeled using automatic-surface-to-surface algorithm. The contact interface force was calculated using the penalty function method with a penalty factor of 0.01. The thickness offset of the shell elements was activated to calculate the thinning or thickening of the wall thickness. The Coulomb friction model was applied to describing the contact frictional behavior between profile and bending die or PVC fillers.

3.4 Hybrid explicit-implicit solvent method

In this study, the dynamic explicit algorithm was utilized for solving the forming process of stretch-bending due to its high computational efficiency and good stability [32]. The unloading springback process was simulated using implicit static algorithm, which is unconditionally stable and can perform the time integration of the equations at arbitrarily large time step [33]. Generally, there are two approaches to solve the unloading springback process, including the seamless implicit analysis (SIA) approach and multi-step implicit analysis (MSIA) approach [34,35]. The former is that the solver can automatically and seamlessly switch from the explicit dynamic algorithm to the implicit static algorithm at the end of forming process simulation, and then run the static springback analysis in one step. The time step was twice that of the forming process analysis. The MSIA approach uses an artificial stabilization method to analyze the springback process within multiple time steps. By artificially introducing a series of springs in the FE model, the spring stiffness decreases gradually during solving process and is removed at the end of the solution. The step number in springback analysis was set to 4 and the initial time step was 0.001. The scale factor for artificial stabilization was set to be 0.004.

4 Results and discussion

4.1 Effect of numerical algorithm and parameter on computational accuracy and efficiency

An accurate FE model is the premise for predicting forming defects in stretch-bending process of hollow profile. The influences of numerical algorithms and parameters, including shell element formulation, NIP, element size, and springback analysis approach, on the computational accuracy and efficiency were systematically evaluated. The basic process conditions used in FE simulations are described as follows: the pre-stretching and post-stretching forces were $A\sigma_0$ (A is the cross-section area of profile); no PVC fillers were added in the cavity of hollow profile. The solutions of FE models were performed on the ThinkStation P510 workstation.

Table 1 shows comparison of computational accuracy and efficiency under different choices of numerical parameters and algorithms. It can be seen that the fully integrated shell element has higher prediction accuracy for cross-section distortion and springback, while the computational time is more than twice that of the Belytschko−Tsay element. The fully integrated shell element has 4 in-plane integration points at each through-thickness location, and the Bathe Dvorkin transverse shear treatment is used to eliminate the w-mode hourglass. Therefore, it has better accuracy in calculating the stress and strain distribution of the shell elements.

NIP has a great influence on the calculation of element stiffness and through-thickness stress. Table 1 presents that the predicted cross-section distortion and springback gradually approximate the experimental values as NIP increases. NIP of 2 is not enough, while NIP of 7 can promote a better solution. And the prediction results stabilize nearly at NIP of larger than 7. During bending, the boundary between elastic and plastic deformation zones on the cross-section of hollow profile, i.e. the

Table 1 Comparison in computational accuracy and efficiency under different choices of numerical parameters and algorithms

Numerical parameter	Element formulation		NIP				Shell element size/mm			Springback analysis approach		Measured value
	Belytschko−Tsay element	Fully integrated shell element	2	7	10	15	2	5	7	SIA	MSIA	
Cross-section distortion/mm	2.84	2.72	2.53	2.72	2.72	2.7	2.72	2.51	2.38	2.87	2.72	2.6
Springback/mm	6.95	7.17	6.89	7.17	7.17	7.16	7.17	7.73	7.87	1.15	7.17	7.4
Computational time/min	42.3	99	47.5	99	123	162	99	54	31	95	99	−

stress discontinuity point, is constantly changing. When the NIP is small, the stress discontinuity point cannot be accurately calculated. It is also worth noting that when the NIP exceeds 7, the computational time increases linearly. The computational time with NIP of 15 is 63.6% longer than that with NIP of 7.

Shell element size is sensitive to the computational accuracy and efficiency. As shown in Table 1, the computational time obviously decreases as the shell element size increases. The computational time using the mesh size of 2 mm is about three times that of the mesh size of 7 mm. The prediction accuracy decreases with increasing element size. The smaller the element size is, the closer the stiffness matrix of FE model is to reality. A higher prediction accuracy can be achieved by choosing the element size of 2 mm.

The predicted cross-section distortion using SIA approach is slightly larger than that using MSIA approach. The springback predicted using the SIA approach is only 1.15 mm, which is obviously deviated from the experimental value (7.4 mm). While the prediction result using MSIA approach is almost the same as the experimental one. This is mainly because the residual stress relaxation of bending profile is more thorough using MSIA approach. For the springback problems with convergence difficulties, the prediction accuracy using MSIA approach is higher. However, its disadvantage is that the springback FE model needs to be re-established based on the deformed meshes, stress and strain of bending profile at the end of the bending stage. Besides, the total computational time is slightly increased.

Considering the computational accuracy and efficiency, the optimal choices of numerical algorithms and parameters in FE modelling were determined as follows: the fully integrated shell element, NIP of 7, shell element size of 2 mm, and multi-step implicit analysis approach. To further validate the rationality of the above choices, the simulated and experimental values of cross-section distortion along the length direction of bending profile were compared in detail (see Fig. 7(a)). It can be seen that the overall trend between the two is in good agreement. The maximum prediction error is located on the middle cross-section of hollow profile, which is approximately 6.7%. Figure 7(b) shows the simulated and experimental values of springback at different pre-stretching forces. The prediction accuracy at larger pre-stretching force is higher than that at smaller pre-stretching force. The maximum prediction error is 7.5% at the pre-stretching force of $0.5A\sigma_0$. When the pre-stretching force is close to $A\sigma_0$, the prediction error is quite small. The slight difference may result from the ignoring of material anisotropy. The established FE model has excellent predictive ability for cross-section distortion and springback, demonstrating that the choices of numerical algorithms and parameters are accurate and reliable.

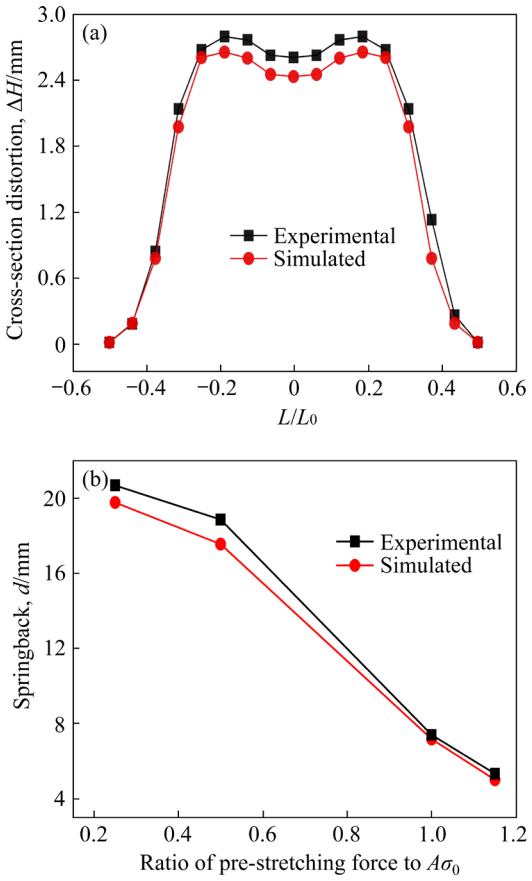

Fig. 7 Comparison between simulated and experimental results: (a) Cross-section distortion along length direction of bending profile; (b) Springback at different pre-stretching forces

4.2 Defect formation mechanisms

4.2.1 Stress distribution on cross-section of aluminum profile

The stress state on the middle cross-section $C1$ (see Fig. 3(a)) of bending profile was analyzed. Figure 8(a) shows the effective and principal stress distribution of shell elements from locations A to B at the end of bending stage when the pre-stretching force was $0.25A\sigma_0$. It can be seen that the principal

stress of the outer material is manifested as the maximum principal stress (tensile stress), while that of the inner material is the minimum principal stress (compressive stress). The second principal stress, i.e. the intermediate principal stress, is approximately zero. Two of the three principal stresses at each shell element are equal to zero. The maximum absolute error between the von Mises stress and principal stress for the inner and outer materials is less than 3%. The stress neutral layer is located at the cross-sectional height of 45 mm, and the type of principal stress at this position is changed. As the overall height of the cross-section is 60.6 mm, the stress neutral layer is shifted obviously towards the inner compression zone during stretch-bending process.

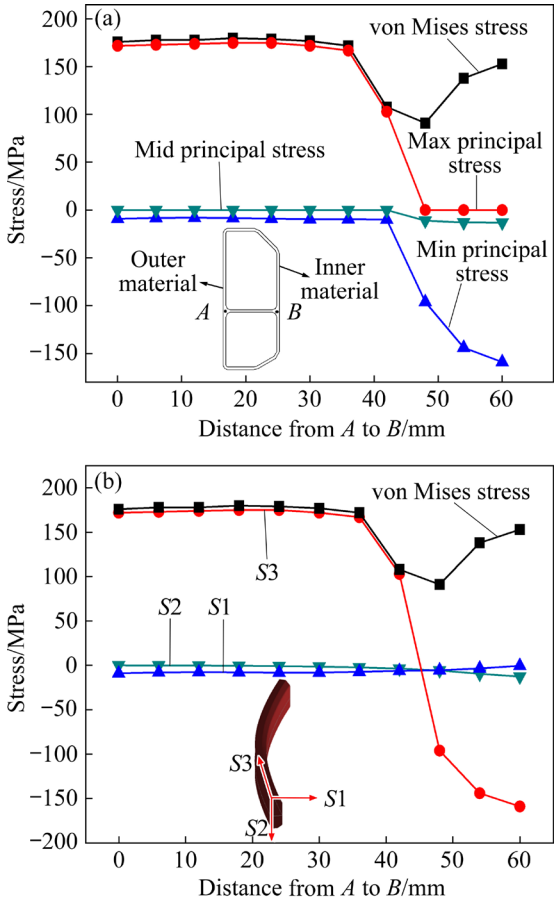

Fig. 8 Stress distribution along height direction of cross-section: (a) Effective and principal stresses; (b) Radial ($S1$), axial ($S2$) and circumferential ($S3$) stresses

To further ascertain the stress state, a cylindrical local coordinate system was established based on the radial, axial and circumferential directions of bending profile. Figure 8(b) shows the distribution of 3D stresses along the height direction of cross-section, where $S1$, $S2$ and $S3$ are the radial, axial and circumferential stresses, respectively. It is clear that the radial and axial stresses are close to zero. The effective stress is basically equal to the absolute value of circumferential stress, and the maximum relative error between two is less than 3%.

Based on the quantitative analysis of effective, principal and 3D stresses in local cylindrical coordinate system, it is concluded that the stress state of profile during the stretch-bending process is uniaxial with only a circumferential stress. The absolute values of effective stress, maximum and minimum principal stresses are basically equal to those of circumferential stress. Thus, the cross-section distortion in stretch-bending is mainly caused by the resultant force of circumferential tensile and compressive stresses in the outer and inner materials. The inconsistent stress state on cross-section produces a reverse moment, which results in the springback of bending profile after unloading the forming tools.

4.2.2 Stress distribution along length direction of bending profile

Figure 9 shows the distribution of circumferential stress and cross-section distortion along the length direction of profile at the end of bending stage. The tensile stress distribution of the outer material is very non-uniform. The maximum tensile stress with a value of 196 MPa is located at the cross-section locations of L/L_0=±0.18, while the minimum tensile stress is located at the center of bending profile. When cross-section location L/L_0 is in the range from −0.18 to 0.18, the distribution characteristic of tensile stress presents a V-shape. When L/L_0>0.18 and L/L_0<−0.18, the closer the deformation region to both ends of the bending profile, the smaller the tensile stress. The distribution of cross-section distortion is significantly influenced by circumferential tensile stress. The cross-section distortion at mid-part of the profile is smaller than that in the region nearby. The maximum cross-section distortion (2.97 mm) is located at the cross-section location of L/L_0=±0.18. The tensile stress at both ends of the profile is larger than that at the mid-part of the profile, but its cross-section distortion is much lower. One reason is that the structural strength of deformation part near both ends of bending profile increases due to the constraints of the main chucks. In addition, the

radial component of circumferential tensile stress at both ends of the profile is relatively small, which is conducive to reducing the cross-section distortion.

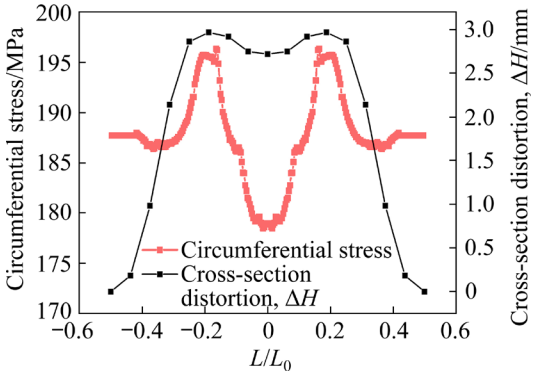

Fig. 9 Circumferential stress and cross-section distortion distribution along length direction of profile

4.3 Effect of unloading process on cross-section distortion

Figure 10 shows the variation of cross-section distortion of hollow profile before and after unloading. It is clear that the cross-section distortion is closely related to the unloading process. After unloading the forming tools, the cross-section distortion along the length direction of the profile decreases obviously. The maximum difference of the cross-section distortion along the length direction of the profile between before and after unloading is up to 13%. Two reasons are related to this variation. Firstly, the cross-section distortion of bending profile includes plastic and elastic deformation. The elastic deformation can be recovered after unloading the forming tools. Secondly, the reverse moment during unloading process produces a reaction force on the bending profile, which can reduce the cross-section distortion.

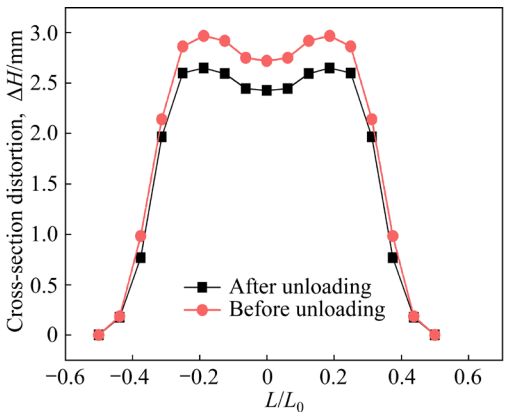

Fig. 10 Effect of unloading process on cross-section distortion of bending profile

4.4 Characteristics of cross-section distortion and springback during partial stretch-bending

Figure 11 shows the strain distribution and deformation pattern of aluminum profile during partial stretch-bending processes. L' is defined as the arc length of the contacting region between the profile and the bending die. When the profile is initially attached to the bending die, the large strain is concentrated on the outer material of bending profile's middle part, while the strain in the inner material is small (see Fig. 11(a)). The deformation in other parts of the profile is basically elastic deformation. As the bending process proceeds, the plastic deformation region gradually extends to both ends of the bending profile, and the maximum plastic strain increases obviously. When the profile is in fully contact with the bending die, the overall regions of profile are basically in the plastic tensile stage, and the strain difference between the inside and outside materials of profile decreases.

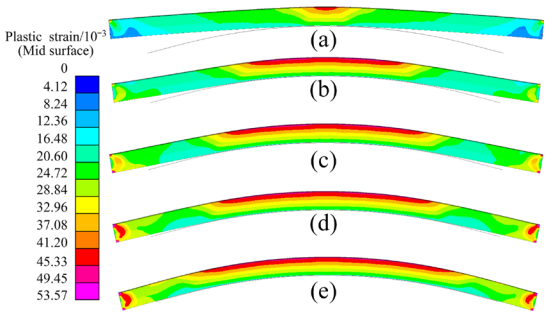

Fig. 11 Strain distribution and deformation pattern of aluminum profile during partial stretch-bending processes: (a) L'=0.3L_0; (b) L'=0.55L_0; (c) L'=0.7L_0; (d) L'=0.8L_0; (e) L'=1.0L_0

Figure 12 shows the characteristics of cross-section distortion and springback after unloading of the partial stretch-bending processes. It can be seen that the cross-section distortion along the length direction of the bending profile is symmetric about the center of bending profile. When L' is less than 0.4L_0, the distribution shows a V-shaped characteristic. From the center to two ends of the bending profile, the cross-section distortion decreases sharply. When L' is larger than 0.4L_0, the distribution presents a W-shaped characteristic. As L' further increases, the maximum cross-section distortion increases obviously. The springback increases gradually with increasing L'. When L' is 0.25L_0, the springback amount is 3.675 mm. The springback amount increases by 95.21% as L'

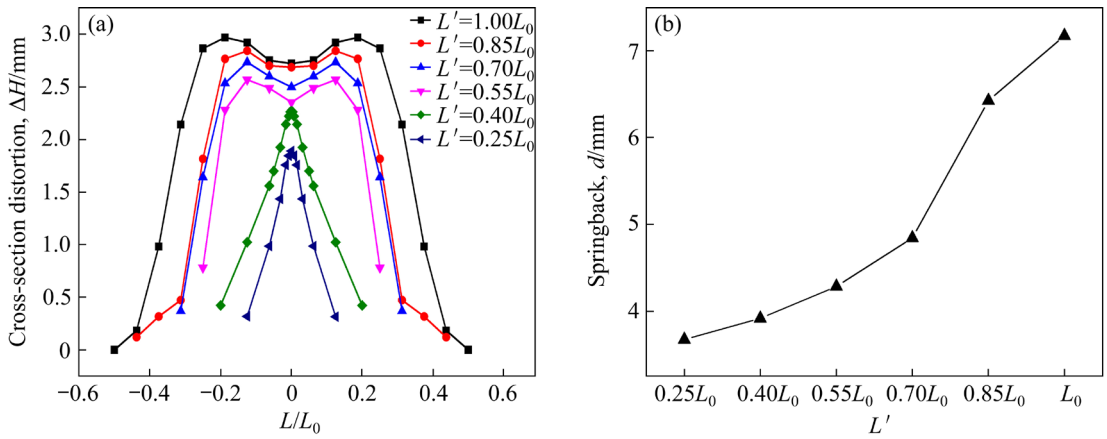

Fig. 12 Characteristics of cross-section distortion and springback after unloading of partial stretch-bending processes: (a) Cross-section distortion; (b) Springback

increases to L_0 due to the increase of elastic deformation amount.

4.5 Effect of pre-stretching force on forming quality

Figure 13 shows the influence of pre-stretching force on forming quality. It is clear that pre-stretching force has a significant impact on the cross-section distortion and springback. When the pre-stretching force is 0, the cross-section distortion and springback are 1.00 and 24.22 mm, respectively. The cross-section distortion increases gradually with increasing pre-stretching force. The springback decreases gradually as pre-stretching force increases to $1.15A\sigma_0$, and then remains unchanged with further increasing pre-stretching force.

The main purpose of applying pre-stretching force is to change the stress distribution on cross-section of bending profile, so as to reduce the springback. Figure 14 shows the circumferential stresses for the inner and outer materials of the bending profile at different pre-stretching forces. When pre-stretching force is less than $0.5A\sigma_0$, the stress neutral layer during the stretch-bending is approximately located at the middle of the cross-section. Compressive and tensile plastic deformation occurs in the interior and exterior of the bending profile, respectively, while elastic deformation occurs in the intermediate region. Therefore, the stress distribution along the height direction of cross-section is seriously nonuniform, resulting in an excessive springback. With the increase of pre-stretching force, the stress neutral layer gradually shifts to the inside of the profile. At pre-stretching

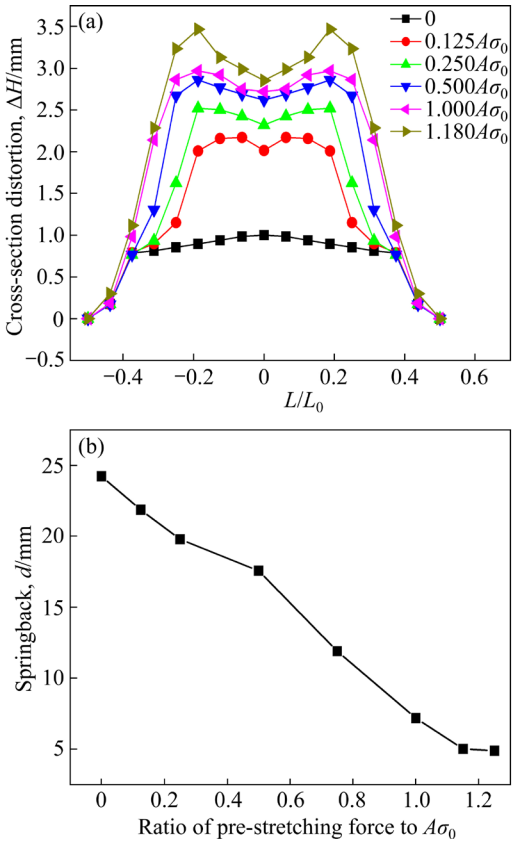

Fig. 13 Influence of pre-stretching force on bending forming quality: (a) Cross-section distortion; (b) Springback

force of $A\sigma_0$, the entire cross-section of bending profile is subjected to tensile stress. Thus, the non-uniform stress distribution on cross-section of the profile is significantly improved, which is conducive to greatly reducing the springback. When the stress neutral layer is completely offset from the innermost side of the bending profile, increasing the pre-stretching force has little effect on reducing

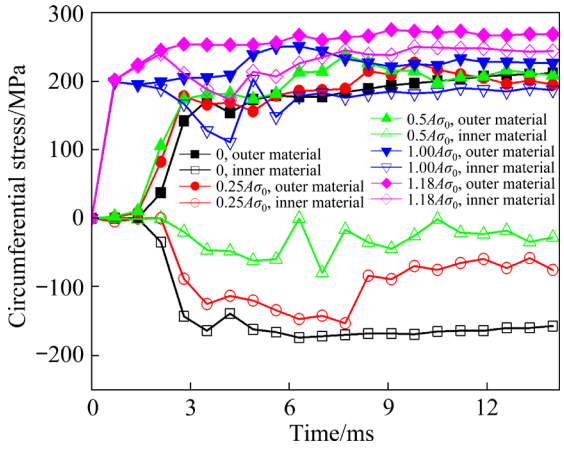

Fig. 14 Variation of circumferential stress for inner and outer materials of bending profile at different pre-stretching forces

springback. Besides, applying excessive pre-stretching force can also cause serious cross-section distortion and wall thickness thinning. The maximum cross-section distortion is 3.467 mm at the pre-stretching force of $1.18A\sigma_0$, which is 16.81% larger than that (2.968 mm) at the pre-stretching force of $A\sigma_0$.

Another important purpose of applying pre-stretching force is to improve anti-demolding and anti-wrinkling abilities of the profile. At low pre-stretching force, there exists large compressive stress at the lower flange of the profile, which induces the profile demoulding and wrinkling (see Fig. 15). The simulation results indicate that when pre-stretching force is less than $0.25A\sigma_0$, the compressive stress of lower flange exceeds 231.67 MPa, and wrinkling instability occurs.

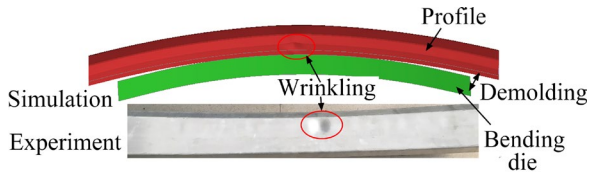

Fig. 15 Schematic diagram showing demolding and wrinkling phenomena at low pre-stretching force

4.6 Effect of post-stretching force on forming quality

Figure 16 shows the influence of post-stretching force on cross-section distortion and springback. With the increase of post-stretching force, the cross-section distortion increases, while the springback first decreases slightly, and then tends to be stable. Figure 17 shows the stress−strain history of the bending profile with applying post-stretching force. In the pre-stretching stage, the whole material of the profile is subjected to plastic tensile stress, and at this time the stress and strain are respectively σ_T and ε_T. In the bending stage, the stress in the outer material continues increase to σ_M under the superposition of tensile stress generated by the bending moment, while the stress in inner material is elastically unloaded to σ_N along the stress−strain history TE under the action of compressive stress. In the post-stretching stage, the stress in the outer material continues to increase to $\sigma_{M'}$, while the stress in the inner material also increases to $\sigma_{N'}$ along the stress−strain history of ET−TM. When the applied post-stretching force ensures that both the inner and outer materials of the bending profile are in a plastic tensile stress state, the springback can be reduced greatly. Further increasing the post-stretching force, the springback is reduced slightly. Compared with the pre-stretching force, the effect of post-stretching force on decreasing springback is limited. Besides, the

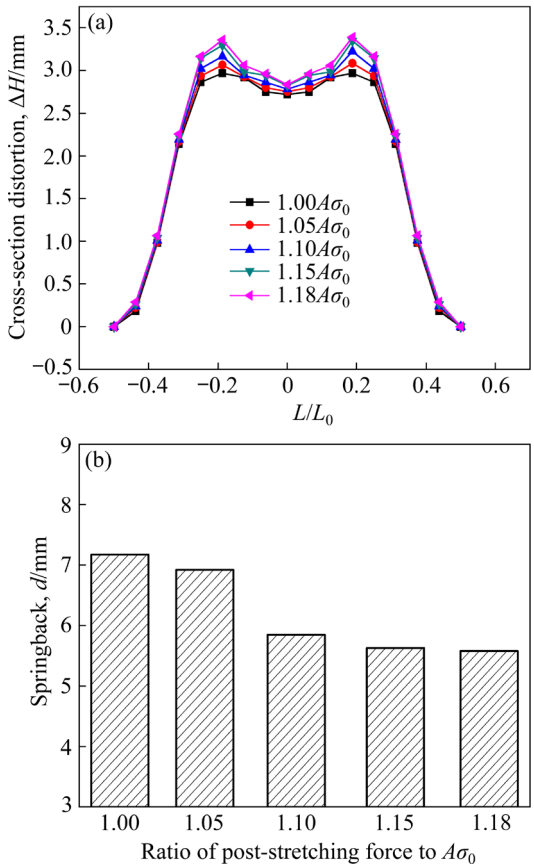

Fig. 16 Influence of post-stretching force on bending forming quality: (a) Cross-section distortion; (b) Springback

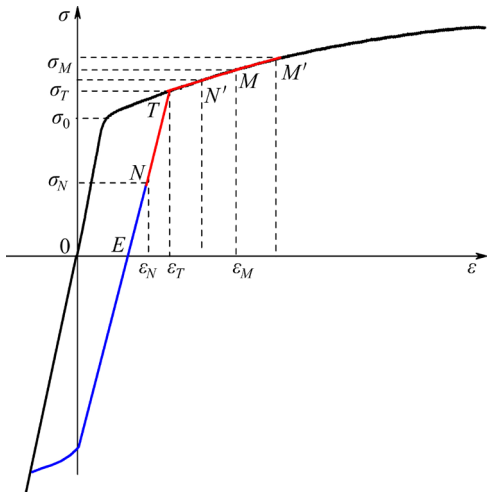

Fig. 17 Stress−strain history of bending profile with applying post-stretching force (M and N respectively represent the elements in outer and inner materials of profile, respectively)

cross-section distortion increases due to the increase of circumferential tensile stress in the outer material.

4.7 Effect of friction between profile and bending die on forming quality

The existence of friction leads to an uneven material flow along the bending die and thus affects the stress distribution of bending profile. Figure 18 shows the influence of friction on cross-section distortion and springback. With the increase of friction coefficient, the cross-section distortion decreases slightly in the deformation region from $-0.25L/L_0$ to $0.25L/L_0$, while it increases in the deformation regions of less than $-0.25L/L_0$ or more than $0.25L/L_0$. Since the maximum cross-section distortion is located in the middle deformation region, properly increasing the friction coefficient can reduce the maximum cross-section distortion to a certain extent. The bending springback gradually increases with increasing friction coefficient. At a large friction force, the axial pre-stretching force is difficult to uniformly transmit along the length direction of the curved profile. As a result, the tensile stress in the middle region of profile decreases, while that in the regions near the two ends of profile increases. In addition, as the friction force increases, the springback amount and direction in each deformation region of bending profile become more inconsistent, increasing the difficulty of springback compensation. Therefore, to improve the forming accuracy of bending profile, lubrication should be exerted between the bending die and the profile to minimize the friction force.

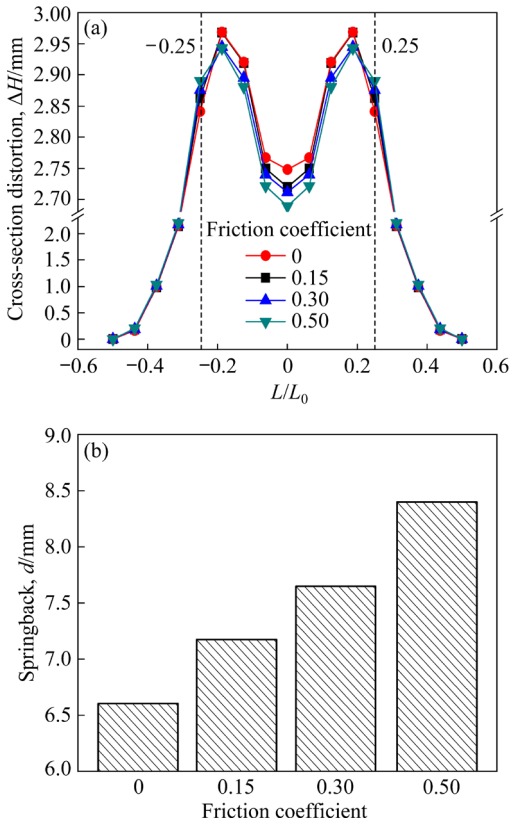

Fig. 18 Effect of friction coefficient on bending forming quality: (a) Cross-section distortion; (b) Springback

4.8 Effect of adding internal fillers on forming quality

Figure 19 shows the effect of adding internal fillers on cross-section distortion and springback of the bending profile. It is clear that adding PVC fillers into the cavities of profile has a strong inhibitory effect on the collapse of upper flange. The maximum collapse magnitude ΔH is only 0.505 mm, which is 83% less than that of the stretch-bending process without adding internal fillers. This is mainly due to the compressive stress exerted by PVC fillers on the inner surface of hollow profile, which increases the ability of the profile to resist radial deformation. As shown in Fig. 19(b), the springback amount for stretch-bending process with adding internal fillers is 20.95 mm, about 192.2% higher than that of stretch-bending process without adding internal fillers (7.17 mm). Figure 20 shows the variation of circumferential stress during the stretch-bending process with and without adding internal fillers. It

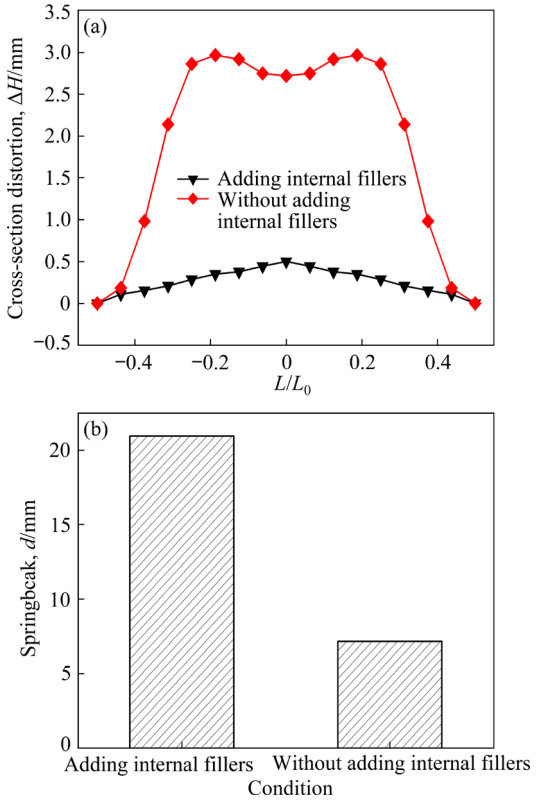

Fig. 19 Effect of adding internal fillers on bending forming quality: (a) Cross-section distortion; (b) Springback

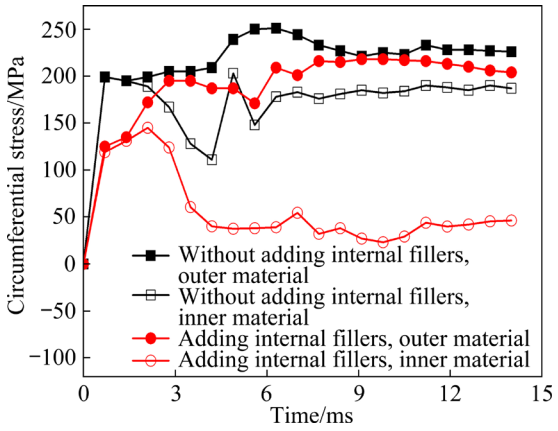

Fig. 20 Variation of circumferential stress during stretch-bending with and without adding internal fillers

can be seen that the outer and inner materials of the profile are closely subjected to plastic tensile stress for stretch-bending without adding internal fillers. After adding internal fillers, the tensile stress of inner material is less than 50 MPa, which is in the state of elastic tensile stress. Thus, the stress gradient on cross-section of hollow profile is larger, resulting in the increase of springback. Besides, the elastic deformation of PVC fillers can be recovered after unloading the forming tools, which further increases the springback of the bending profile. In the actual operation, the circumferential stress distribution along the length direction of profile is seriously non-uniform due to the inconsistency of contact clearance between PVC fillers and hollow profile, which is unfavorable for achieving accurate stretch-bending.

5 Conclusions

(1) Considering the computational accuracy and efficiency, the optimal choices of numerical algorithms and parameters in FE modelling were determined as follows: the fully integrated shell element, NIP of 7, shell element size of 2 mm and multi-step implicit analysis approach.

(2) The stress state of profile in stretch-bending process is uniaxial with only a circumferential stress. The stress distribution along the length direction of bending profile is non-uniform and the maximum tensile stress is located at a certain distance away from the center of bending profile. As aluminum profile is gradually attached to bending die, the distribution characteristic of cross-section distortion along the length direction of bending profile changes from V-shape to W-shape. After unloading the forming tools, cross-section distortion decreases obviously due to the stress relaxation, with a maximum difference of 13% between before and after unloading.

(3) When pre-stretching and post-stretching forces increase, cross-section distortion increases gradually, while springback first decreases and then remains unchanged. At low pre-stretching force, demoulding and wrinkling instability in bending profile occur due to the large compressive stress at the lower flange of the profile. Compared with the pre-stretching force, the role of pre-stretching force in decreasing springback is limited.

(4) With increasing friction between the bending die and the profile, cross-section distortion slightly decreases, while springback increases. Cross- section distortion decreases by 83% with adding PVC fillers into the cavities of the profile, while springback increases by 192.2%.

CRediT authorship contribution statement

Zhi-wen LIU: Methodology, Data curation, Supervision, Visualization, Funding acquisition,

Writing − Original draft; **Zi-xuan DONG:** Software, Investigation, Analysis; **Cong-chang XU:** FE modeling, Investigation; **Jie YI:** Resources, Supervision, Experiment validation; **Luo-xing LI:** Conceptualization, Methodology, Resources, Writing − Review & editing, Funding acquisition.

Declaration of competing interest

The authors declare that they have no known competing financial interests or personal relationships that could have appeared to influence the work reported in this paper.

Acknowledgments

This work was supported by the National Natural Science Foundation of China (Nos. 52005244, U20A20275), the Natural Science Foundation of Hunan Province, China (Nos. 2021JJ30573, 2023JJ60193), and the Open Fund of State Key Laboratory of Advanced Design and Manufacture for Vehicle Body, China (No. 31715011)

References

[1] YI J, WANG G, LI S K, LIU Z W, GONG Y L. Effect of post-weld heat treatment on microstructure and mechanical properties of welded joints of 6061-T6 aluminum alloy [J]. Transactions of Nonferrous Metals Society of China, 2019, 29(10): 2035−2046.

[2] GENG H C, WANG Y L, ZHU B, WANG Z J, ZHANG Y S. Effect of solution treatment time on plasticity and ductile fracture of 7075 aluminum alloy sheet in hot stamping process [J]. Transactions of Nonferrous Metals Society of China, 2022, 32(11): 3516−3533.

[3] LIU Z W, WANG G, YI J. Study on heat transfer behaviors between Al−Mg−Si alloy and die material at different contact conditions based on inverse heat conduction algorithm [J]. Journal of Materials Research and Technology, 2020, 9(2): 1918−1928.

[4] SHENG X F, HE C X, CHENG Y J, RAO X X, HE G A. New method and mechanism for quickly obtaining quenching sensitivity temperature range of 7055 aluminum alloy [J]. Transactions of Nonferrous Metals Society of China, 2023, 33(1): 36−45.

[5] YI J, WANG Z H, LIU Z W, ZHANG J M, HE X. FE analysis of extrusion defect and optimization of metal flow in porthole die for complex hollow aluminium profile [J]. Transactions of Nonferrous Metals Society of China, 2018, 28(10): 2094−2101.

[6] YI J, LIU Z W, ZENG W Q. Isothermal extrusion speed curve design for porthole die of hollow aluminium profile based on PID algorithm and finite element simulations [J]. Transactions of Nonferrous Metals Society of China, 2021, 31(7): 1939−1950.

[7] LIU Z, LI L, LI S, YI J, WANG G. Simulation analysis of porthole die extrusion process and die structure modifications for an aluminum profile with high length–width ratio and small cavity [J]. Materials, 2018, 11(9): 1517.

[8] LIU Z W, YI J, LI S K, NIE W J, LI L X, WANG G. Study on inhomogeneous cooling behavior of extruded profile with unequal and large thicknesses during quenching using thermo-mechanical coupling model [J]. Transactions of Nonferrous Metals Society of China, 2020, 30(5): 1211−1226.

[9] VOLLERTSEN F, SPRENGER A, KRAUS J, ARNET H. Extrusion, channel, and profile bending: a review [J]. Journal of Materials Processing Technology, 1999, 87(1/2/3): 1−27.

[10] WANG M, LU G L, CAI Z Y, LI M Z. Research on continuous roll forming for manufacturing 3D curved surface parts with variable transverse curvatures [J]. Journal of Manufacturing Processes, 2018, 36: 459−464.

[11] LU K, ZOU T, LUO J, LI D, PENG Y. Stretch bending process design by machine learning [J]. The International Journal of Advanced Manufacturing Technology, 2022, 120(1): 781−799.

[12] TRONVOLL S A, MA J, WELO T. Deformation behavior in tube bending: A comparative study of compression bending and rotary draw bending [J]. The International Journal of Advanced Manufacturing Technology, 2023, 124(3/4): 801−816.

[13] LIU Z, LI L, WANG G, CHEN J, YI J. Springback behaviors of extruded 6063 aluminum profile in subsequent multi-stage manufacturing processes [J]. The International Journal of Advanced Manufacturing Technology, 2020, 109(1): 1−13.

[14] EL-DOMIATY A A, ELSHARKAWY A A. Stretch-bending analysis of U-section beams [J]. International Journal of Machine Tools and Manufacture, 1998, 38(1): 75−95.

[15] ZHU H, STELSON K A. Distortion of rectangular tubes in stretch bending [J]. Journal of Manufacturing Science and Engineering, 2002, 124(4): 886−890.

[16] CORONA E. A simple analysis for bend-stretch forming of aluminum extrusions [J]. International Journal of Mechanical Sciences, 2004, 46(3): 433−448.

[17] YU C L, LI X Q. Theoretical analysis on springback of L-section extrusion in rotary stretch bending process [J]. Transactions of Nonferrous Metals Society of China, 2011, 21(12): 2705−2710.

[18] ZHAO J, ZHAI R X, QIAN Z P, MA R. A study on springback of profile plane stretch–bending in the loading method of pretension and moment [J]. International Journal of Mechanical Sciences, 2013, 75: 45−54.

[19] ZHAI R X, DING X H, YU S M, WANG C G. Stretch bending and springback of profile in the loading method of prebending and tension [J]. International Journal of Mechanical Sciences, 2018, 144: 746−764.

[20] MA J, WELO T. Analytical springback assessment in flexible stretch bending of complex shapes [J]. International Journal of Machine Tools and Manufacture, 2021, 160: 103653.

[21] MILLER J E, KYRIAKIDES S, BASTARD A H. On bend-stretch forming of aluminum extruded tubes—I: Experiments [J]. International Journal of Mechanical Sciences, 2001, 43(5): 1283−1317.

[22] LIU T J, WANG Y J, WU J J, XIA X J, WANG J B, WANG W, WANG S H. Springback analysis of Z & T-section 2196-T8511 and 2099-T83 Al−Li alloys extrusions in displacement controlled cold stretch bending [J]. Journal of Materials Processing Technology, 2015, 225: 295−309.
[23] CLAUSEN A H, HOPPERSTAD O S, LANGSETH M. Stretch bending of aluminium extrusions for car bumpers [J]. Journal of Materials Processing Technology, 2000, 102(1/2/3): 241−248.
[24] LIU T J, XIA X J, WU W C, YIN C J, WANG Y J, TIAN H F, KONG W C. Experimental investigations for electric heating rotary stretch bending process of extruded Ti−6Al−4V alloy profile with T-section [J]. Procedia Engineering, 2017, 207: 747−752.
[25] LIU T J, WANG Y J, WU J J, XIA X J, WANG J B, LI S L, WANG S H, WANG J , HAN G. Minimum bending radius of Al−Li alloy extrusions in stretch bending [J]. Proceedings of the Institution of Mechanical Engineers, Part B: Journal of Engineering Manufacture, 2018, 232(2): 281−295.
[26] PAULSEN F, WELO T. Application of numerical simulation in the bending of aluminium-alloy profiles [J]. Journal of Materials Processing Technology, 1996, 58(2/3): 274−285.
[27] HOPPERSTAD O S, BERSTAD T, ILSTAD H, LADEMO O G, LANGSETH M. Effects of the yield criterion on local deformation in numerical simulation of profile forming [J]. Journal of Materials Processing Technology, 1998, 80: 551−555.
[28] GU Z W, LÜ M M, LI X, XU H. Stretch bending of Z-section stainless steel profile [J]. Journal of Iron and Steel Research: International, 2016, 23(6): 525−530.
[29] LIU C G, ZHANG X G, WU X T, ZHENG Y. Optimization of post-stretching elongation in stretch bending of aluminum hollow profile [J]. The International Journal of Advanced Manufacturing Technology, 2016, 82(9/10/11/12): 1737−1746.
[30] LIANG J, CHEN C, LI Y, LIANG C. Effect of roller dies on springback law of profile for flexible 3D multi-point stretch bending [J]. The International Journal of Advanced Manufacturing Technology, 2020, 108: 3765−3777.
[31] GU Z W, JIA L, LI X, ZHU L J, XU H, YU G. Stretch bending defect control of L-section SUS301L stainless-steel components with variable contour curvatures [J]. Journal of Iron and Steel Research International, 2019, 26: 1376−1384.
[32] OLEKSIK V, PASCU A, ROCA L, BONDREA I. Numerical-experimental comparison study regarding single point incremental forming process [J]. American Institute of Physics, 2013, 1532(1): 532−537.
[33] LAJARIN S F, MARCONDES P V P. Influence of computational parameters and nonlinear unloading behavior on springback simulation [J]. Journal of the Brazilian Society of Mechanical Sciences and Engineering, 2013, 35(2): 123−129.
[34] WANG G, ZHU G, KOU L, LI T, LIU Z, SHANG X, JIANG X, ZHU X. Effect of heat treatment conditions on stamping deformation and springback of 6061 aluminum alloy sheets [J]. Materials Research Express, 2020, 7(1): 016512.
[35] WANG G, LI T, KOU L Y, ZHU G G, ZHU X J, SHANG X, LIU Z W. Influence of artificial aging time on bending characteristics of 6061 aluminum sheet [J]. Materialwissenschaft und Werkstofftechnik, 2020, 51(11): 1533−1542.

双腔铝型材力控制模式拉弯条件下的截面畸变及回弹特性

刘志文[1,2]，董子轩[1]，徐从昌[2]，易 杰[2]，李落星[2]

1. 南华大学 机械工程学院，衡阳 421001；
2. 湖南大学 整车先进设计制造技术国家重点实验室，长沙 410082

摘 要：采用显−隐式混合方法建立了用于模拟双腔铝型材力控制模式拉弯工艺成形过程的三维弹塑性有限元模型。考虑到计算的准确性和效率，给出了有限元建模中各种数值参数和算法的最优选择。揭示了型材拉弯截面畸变和回弹的形成机理，系统研究了预拉伸、补拉伸、摩擦和添加内填充物对弯曲成形质量的影响。结果表明，铝型材拉弯时的应力状态为单轴环向应力。应力沿型材长度方向分布不均匀，且最大拉应力位于离型材中心一定距离的位置；随着型材逐渐包覆到弯曲模具上，沿型材长度方向的截面畸变分布特征由 V 形转变为 W 型。成形工具卸载后，由于应力释放截面畸变明显减小，卸载前后畸变最大差值为 13%。随着预拉伸力和补拉伸力的增加，截面畸变逐渐增加，而回弹先减小后保持不变。增加弯曲模具与型材间的摩擦，截面畸变略微减小，但回弹增大。往型材型腔中添加 PVC 填充物，型材拉弯截面畸变减小了 83%，但回弹增大了 192.2%。

关键词：空心铝型材; 力控制模式拉弯; 数值参数; 回弹分析法; 截面畸变; 回弹; 工艺参数

(Edited by Wei-ping CHEN)